

# Reconstructing the Assembly of Massive Galaxies. III: Quiescent Galaxies Lose Angular Momentum as They Evolve in a Mass-dependent Fashion.

ZHIYUAN JI<sup>1</sup> AND MAURO GIAVALISCO<sup>2</sup>

<sup>1</sup>*Steward Observatory, University of Arizona, 933 N. Cherry Avenue, Tucson, AZ 85721, USA*

<sup>2</sup>*University of Massachusetts Amherst, 710 North Pleasant Street, Amherst, MA 01003-9305, USA*

## ABSTRACT

We study the evolution of stellar kinematics of a sample of 952 massive quiescent galaxies with  $M_* > 10^{10.5} M_\odot$  at  $0.6 < z < 1$ . Utilizing spatially integrated spectroscopy from the LEGA-C survey, we focus on the relationship between the observed integrated stellar velocity dispersion ( $\sigma'_{\text{star}}$ ) and the morphological axial ratio ( $q$ ), and its variation with the stellar age and mass of quiescent galaxies. For the youngest quiescent galaxies, regardless of stellar mass,  $\sigma'_{\text{star}}$  decreases with increasing  $q$ , a trend that is consistent with a system having significant rotation and hence suggests that massive galaxies still retain significant amount of angular momentum in the aftermath of quenching. As they continue to evolve, the variation of the  $\sigma'_{\text{star}}-q$  relationship depends on stellar mass. For quiescent galaxies with  $M_* < 10^{11.3} M_\odot$ ,  $\sigma'_{\text{star}}$  decreases with  $q$  in all stellar-age bins, suggesting that the quiescent populations of this mass regime retain significant rotation even long time after quenching. In contrast, for more massive quiescent galaxies with  $M_* > 10^{11.3} M_\odot$ , the relationship between  $\sigma'_{\text{star}}$  and  $q$  becomes significantly flattened with increasing stellar age. This indicates that, as the very massive galaxy populations continue to evolve after quenching, angular momentum gradually reduces, which eventually transforms them into velocity-dispersion supported systems. We suggest that incoherent, continuous merging and accretion events onto the galaxies are the main drivers of the observed mass-dependent, post-quenching dynamical evolution, because more massive galaxies are more likely to undergo such interactions. We are witnessing the early formation epoch of fast and slow rotators at  $z \sim 0.8$ , when the Universe was only half of its age nowadays.

*Keywords:* Galaxy formation(595); Galaxy evolution(594); Galaxy structure(622); High-redshift galaxies(734)

## 1. INTRODUCTION

Early type/quiescent galaxies that no longer actively form stars dominate the cosmic stellar-mass budget in the present-day Universe (Muzzin et al. 2013). At redshift  $z \sim 0$ , integral-field spectroscopic (IFS) observations revealed a bimodal distribution in the stellar kinematics of massive quiescent galaxies (Emsellem et al. 2004, 2007; Cappellari et al. 2007). Two classes – fast and slow rotators – are identified to have distinct  $V/\sigma$ , i.e. the ratio of the ordered ( $V$ ) to random ( $\sigma$ ) motions in a stellar system. Relative to fast rotators, slow rotators have lower  $V/\sigma$ , and they generally are more mas-

sive with stellar masses of  $M_* \gtrsim 10^{11.3} M_\odot$  and weakly triaxial (Cappellari 2016). Constraining the pathway to establishing the observed kinematical dichotomy at  $z \sim 0$  is the key for understanding the assembly of massive galaxies, which requires us to push the study of stellar kinematics in quiescent galaxies towards higher redshifts, i.e. closer to the epoch when the dichotomy was emerging.

For quiescent galaxies at high redshifts, however, measuring stellar kinematics with spatially resolved spectroscopy is very challenging, owing to their compact morphologies (e.g. van der Wel et al. 2014; Ji et al. 2024), and the lack of strong emission lines. Prior to the launch of James Webb Space Telescope (JWST, Gardner et al. 2023), such measurements only exist for a handful of rare, extremely bright quiescent galaxies whose observed fluxes are highly magnified due to strong grav-

itational lensing (Newman et al. 2015; Toft et al. 2017; Newman et al. 2018). The immense gain of JWST in sensitivity and angular resolution at IR wavelengths now enables spatially resolved spectroscopy of more general populations (e.g., unlensed) of high- $z$  quiescent galaxies (D’Eugenio et al. 2023). However, such observations are still time-consuming, requiring  $\gtrsim 10$  hours on-source exposure with NIRSpec/IFS (Jakobsen et al. 2022) for a single fairly bright ( $K < 22.5$  mag,  $M_* \sim 10^{11} M_\odot$ ) quiescent galaxy (Nanayakkara et al. 2022). This makes it not possible – even with JWST – to measure stellar kinematics with spatially resolved spectroscopy in statistically large samples of high- $z$  quiescent galaxies on a rapid timescale.

Yet, notwithstanding the very limited sample size of high- $z$  quiescent galaxies with robust measures of stellar kinematics, the findings from existing studies are somewhat surprising. All systems that have been studied show rapid rotation (Newman et al. 2015; Toft et al. 2017; Newman et al. 2018; D’Eugenio et al. 2023), despite that their large stellar mass, i.e. typically  $\gtrsim 10^{11.3} M_\odot$ , suggests that they should be the progenitors of  $z \sim 0$  slow rotators. If those systems are good representative of the underlying population of high- $z$  massive quiescent galaxies, the implication will be profound: Significant dynamical transformations, particularly the loss of angular momentum, must happen after the quenching of massive galaxies. Unfortunately, such an implication can be fraught with systematic errors, considering that the current sample size is rather small and the sample selection function can be complex for observations on target basis.

In this work, instead of relying on spatially resolved spectroscopy, we investigate the dynamical transformation of quiescent galaxies using spatially integrated/unresolved stellar kinematics. In such a way we are able to conduct the analysis with a statistically significant sample of  $\approx 1000$  massive quiescent galaxies at  $z \sim 0.8$ , about half the Hubble time of the Universe today. In particular, we focus on the stellar-age dependence of the empirical relationship between  $\sigma'_{\text{star}}$ <sup>1</sup>, i.e. the observed integrated stellar velocity dispersion (after taking into account the instrumental resolution), and  $q$ , i.e. the ratio of the semi-minor to semi-major axes of the morphology of galaxies which is a sensitive probe of inclination. The idea is illustrated in Figure 1 and described in detail in what follows.

<sup>1</sup> Following the notation of the LEGA-C survey, we use  $\sigma'_{\text{star}}$  to differentiate it from the intrinsic stellar velocity dispersion  $\sigma_{\text{star}}$  commonly used in the literature.

For spatially integrated spectroscopy, both random and ordered (if present) motions contribute to the broadening of intrinsic stellar templates. Therefore,  $\sigma'_{\text{star}}$  equals to the square root of the quadratic sum of the intrinsically random motion ( $\sigma$ ) and the contribution from projected rotation along the line of sight ( $\sigma_{\text{rotation}}$ ). For a system with significant rotation, because  $\sigma_{\text{rotation}}$  decreases with increasing  $q$  (from edge-on to face-on),  $\sigma'_{\text{star}}$  decreases with increasing  $q$  (black solid line in Figure 1). In contrast, for a system dominated by random motion, because the contribution from  $\sigma_{\text{rotation}}$  to  $\sigma'_{\text{star}}$  is negligible compared to  $\sigma$ , a much weaker relationship between  $\sigma'_{\text{star}}$  and  $q$  is expected. A very similar idea<sup>2</sup> has been discussed and utilized in an earlier study by Belli et al. (2017) of a much smaller sample of 24 quiescent galaxies at  $z \sim 2$ .

With spectral energy distribution (SED) modeling growing in sophistication and accuracy, statistically reconstructing high-fidelity star formation histories (SFHs) is becoming possible for high- $z$  massive galaxies when high-quality, panchromatic data are available. The flexibility of the SFH treatment in SED modeling ensures a much less biased, if at all, inference of physical parameters (Carnall et al. 2019; Leja et al. 2019). Built upon this latest development in SED modeling, in the first two papers of this series (Ji & Giallisco 2022a,b), we have utilized the fully Bayesian SED fitting code PROSPECTOR (Johnson et al. 2021) to reconstruct the nonparametric SFH of massive galaxies at  $z \sim 2$ . Combining together the SFHs and morphological analysis, we were able to reconstruct the timing sequence of the morphological transformation of massive galaxies as they evolve from the main sequence to quiescence.

In this third paper, we focus on the dynamical transformation of quiescent galaxies in approximately the last half of the Hubble time. With robust stellar-age estimates from SED fitting, we study the dependence of the relationship between  $\sigma'_{\text{star}}$  and  $q$  on the stellar age of galaxies. Any significant change of the  $\sigma'_{\text{star}}$  vs.  $q$  relationship with stellar age is an indication of strong evolution in the dynamical state of massive galaxies after they quench. The redshift range considered here is  $0.6 < z < 1$ , where statistically significant samples of quiescent galaxies with unresolved stellar kinematics are available. Throughout this paper, we adopt the AB magnitude system and the  $\Lambda$ CDM cosmology

<sup>2</sup> Instead of  $\sigma'_{\text{star}}$ , Belli et al. (2017) studied the relationship between  $q$  and the dynamical mass of galaxies,  $M_{\text{dyn}}$  whose estimation heavily depends on  $\sigma'_{\text{star}}$  measured from the spatially integrated stellar kinematics.

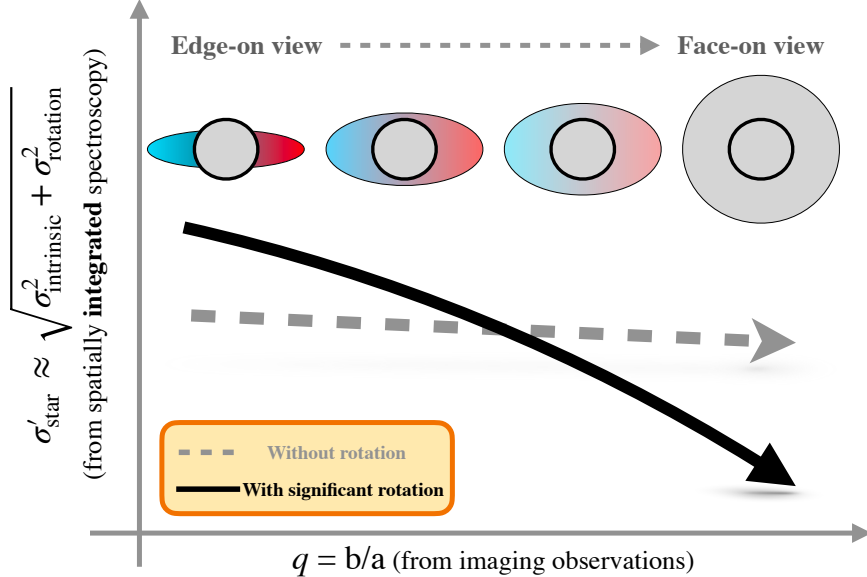


**Figure 1.** Illustration of the main idea of this work (see Section 1 for details). We investigate the dynamical transformation of massive quiescent galaxies at high redshifts with spatially integrated/unresolved stellar kinematics by studying the empirical relationship between  $\sigma'_{\text{star}}$  ( $y$ -axis) and  $q$  ( $x$ -axis).

with Planck Collaboration et al. 2020 parameters, i.e.,  $\Omega_m = 0.315$  and  $h = H_0/(100 \text{ km s}^{-1} \text{ Mpc}^{-1}) = 0.673$ .

## 2. THE SAMPLE

The parent sample considered in this study comes from the Large Early Galaxy Astrophysics Census (LEGA-C, van der Wel et al. 2016; Straatman et al. 2018), the latest and final Data Release 3 (van der Wel et al. 2021). The LEGA-C survey is an ESO/Very Large Telescope public survey that observed with deep spectroscopy (median S/N  $\sim 15$  at 4000 Å) for a sample of  $\sim 3500$  galaxies at  $0.6 < z < 1$ , selected using the  $K$ -band flux from the COSMOS/UltraVISTA survey (Muzzin et al. 2013). Here we only focus on the galaxies with  $M_* > 10^{10.5} M_\odot$ , to ensure (1) good stellar mass completeness (see Figure A1 of van der Wel et al. 2021) and (2) that the environmental effects – external to the host halo of a galaxy – on the evolution of galaxies are minor (e.g. Ji et al. 2018).

We refine the sample selection using the flags from the LEGA-C data release. We require `FLAG_MORPH = 0`, to ensure that during observations the light through the slit is from a single galaxy with a regular morphology, meaning that mergers and galaxies whose LEGA-C spectra are contaminated by adjacent galaxies are excluded from the sample. We also require `FLAG_SPEC = 0`, to exclude the galaxies with clear AGN presence identified by either IR or X-ray observations. These two constraints together ensure the high-quality spectral measures, and eliminate the cases when the interpretation

of the dynamical measures becomes complicated. We cross match the LEGA-C catalog with the photometric catalog of COSMOS2020 (Weaver et al. 2022), and finally select quiescent galaxies using the UVJ criteria of Muzzin et al. (2013). Our final sample contains 952 UVJ-selected quiescent galaxies.

## 3. MEASUREMENTS

### 3.1. $\sigma'_{\text{star}}$ and $q$

The measurements of unresolved stellar kinematics  $\sigma'_{\text{star}}$  and morphological axis ratio  $q$  are taken directly from the LEGA-C data release (Bezanson et al. 2018a; van der Wel et al. 2021). We refer readers to those references for technical details.

Briefly,  $q$  is derived from the HST/ACS  $I_{814}$  imaging in the COSMOS field, following van der Wel et al. (2012) who used the GALFIT package (Peng et al. 2010) to model the 2D light distribution of galaxies assuming a single Sérsic profile.  $\sigma'_{\text{star}}$  were measured with the PPFX package (Cappellari 2017) by fitting the observed spatially integrated spectra with the combination of (1) high-resolution ( $R = 10000$ ) theoretical single stellar templates and emission lines at the instrumental resolution, (2) a 3rd-order multiplicative polynomial and (3) an additive polynomial. The unresolved stellar velocity dispersion  $\sigma'_{\text{star}}$  and gas velocity dispersion are estimated independently by broadening the templates with Gaussian kernels.

### 3.2. SED fitting with Prospector

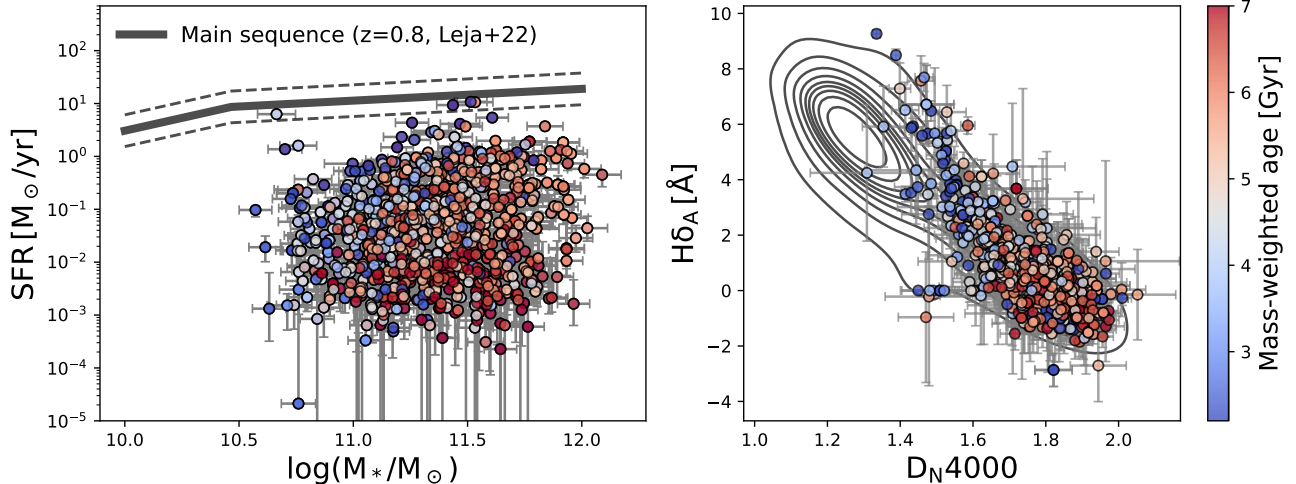


**Figure 2. Left:** Distribution of the final sample of 952 massive quiescent galaxies in the plane of SFR vs  $M_*$ . The black solid line shows the star-forming main sequence of [Leja et al. \(2022\)](#), and the black dashed lines mark the range of  $\pm 0.3$  dex. **Right:** Distribution of the final sample in the plane of  $H\delta_A$  vs.  $D_{N4000}$ . The background grey contours show the distribution of all galaxies with  $M_* > 10^{10.5} M_\odot$  from the LEGA-C survey. Each one of the quiescent galaxies in our final sample is color coded according to its mass-weighted stellar age derived from SED fitting assuming non-parametric SFH. Our quiescent sample selected via UVJ technique also occupies the region of the parameter space of quiescent galaxies in these two planes.

The properties of the stellar-populations of the sample galaxies are derived by fitting the multi-band photometry from the COSMOS2020 catalog with the fully Bayesian code PROSPECTOR ([Johnson et al. 2021](#)). Each one of the sample galaxies has  $\approx 40$  band photometry that densely samples the rest-frame UV-to-NIR wavelengths. Compared to previous COSMOS catalogs, COSMOS2020 includes the new, significantly deeper optical and NIR imaging from the Subaru/HSC and VISTA/VIRCAM surveys ([Weaver et al. 2022](#)). Two catalogs using different aperture photometric methods are available in the COSMOS2020 release, namely the CLASSIC and FARMER catalogs. By default, we use the former where aperture-matched photometry was carried out following [Laigle et al. \(2016\)](#). We note, however, that the difference between the two photometric catalogs is negligible for galaxies in the magnitude range ( $K < 21.5$  mag) considered here (Figure 8 and 9 in [Weaver et al. 2022](#)).

The basic setups of our PROSPECTOR fitting are essentially the same as those in the first two papers of this series ([Ji & Giavalisco 2022a,b](#)). We adopt the Flexible Stellar Population Synthesis (FSPS) code ([Conroy et al. 2009; Conroy & Gunn 2010](#)) where the stellar isochrone libraries MIST ([Choi et al. 2016; Dotter 2016](#)) and the stellar spectral libraries MILES ([Falc3n-Barroso et al. 2011](#)) are used. We assume the [Kroupa \(2001\)](#) initial mass function and the [Byler et al. \(2017\)](#) nebular emission model. We assume the [Calzetti et al. 2000](#) dust attenuation law and fit the V-band dust op-

tical depth with a uniform prior  $\tau_V \in (0, 2)$ . We fix the redshift to the spectroscopically-measured values from LEGA-C, and set the stellar metallicity as a free parameter with a uniform prior in the logarithmic space  $\log(Z_*/Z_\odot) \in (-2, 0.19)$ , where the upper limit of the prior is chosen because it is the highest metallicity that the MILES library covers.

We use the nonparametric form of SFH that is critical for unbiased inference of stellar-population properties (e.g. [Leja et al. 2019](#)). Specifically, we use a piecewise step function composed of nine lookback time bins, where the star formation rate (SFR) is constant within each bin. We fix the first two bins as 0–30 and 30–100 Myr to capture recent episodes of star formation. We also fix the last bin as  $0.9t_H - t_H$  where  $t_H$  is the Hubble Time of observation. The remaining six bins are evenly spaced in the logarithmic lookback time between 100 Myr and  $0.9t_H$ .

To ensure the convergence of nonparametric SFH reconstructions and reasonable uncertainty estimations (e.g. [Carnall et al. 2019; Leja et al. 2019](#)), we adopt the Dirichlet prior ([Leja et al. 2017](#)) during the PROSPECTOR SED fitting. This prior has been demonstrated to be able to recover the diverse shape of SFHs ([Leja et al. 2019](#)). Moreover, using the synthetic observations of simulated galaxies that have similar data quality like the ones we use here for the LEGA-C galaxies, [Ji & Giavalisco \(2022a, see their Appendix A\)](#) demonstrated that the Dirichlet prior can better recover the stellar age of high- $z$  quiescent galaxies compared to

other commonly-used priors, such as the continuity one, which is commonly adopted to measure the SFH of star-forming galaxies.

In Figure 2, we show the distributions of the sample galaxies in the planes of SFR vs.  $M_*$ , and of  $H\delta_A$  (Worthey et al. 1994; Worthey & Ottaviani 1997) vs.  $D_N4000$  (4000Å break, Balogh et al. 1999). From the left panel of the Figure it is immediately clear that the UVJ-selected quiescent galaxies also occupy the parameter space of galaxies below the star-forming main sequence, i.e. with depressed SFR at any given stellar mass. This shows very good consistency among different selection methods of quiescent galaxies.

In the right panel of Figure 2, each one of the galaxies is color coded according to mass-weighted stellar age. It has been extensively shown that  $H\delta_A$  and  $D_N4000$  are sensitive diagnostics of galaxy’s stellar age (e.g. Kauffmann et al. 2003). As the Figure shows, galaxies with lower SFR (at fixed  $M_*$ ), larger  $D_N4000$  and larger (negative)  $H\delta_A$  also have larger ages (older stellar populations) from our PROSPECTOR fitting, demonstrating the robustness of our stellar-age inference. Because the main conclusion of this study depends on the stellar-age measures, in Appendix A we conduct a number of further tests on the robustness of the age inference. We conclude that the our stellar-age measures are robust.

#### 4. RESULTS

We now present the relationship between  $\sigma'_{\text{star}}$  and  $q$ , i.e. the core of this study. We first divide the sample into the low-mass and high-mass subsamples using  $M_* = 10^{11.3}M_\odot$ , i.e. the characteristic mass to separate fast and slow rotators at  $z \sim 0$  (Cappellari 2016). We then further divide each subsample into three subgroups using the 33th- and 67th- percentiles of the stellar-age distribution of the entire quiescent sample.

##### 4.1. The median trend

We measure the median relationship between  $\sigma'_{\text{star}}$  and  $q$  of each one of the subgroups using the Locally Weighted Scatterplot Smoothing (LOWESS<sup>3</sup>) method that fits a smoothed curve to data points through a non-parametric approach, i.e. the process does not require to assume any specific functional form. We estimate the uncertainty of the median relationship via Monte Carlo simulations. In particular, we use Gaussian distributions to resample the individual  $\sigma'_{\text{star}}$  and  $q$  measures with their corresponding uncertainties. We then use LOWESS to measure the median  $\sigma'_{\text{star}}$  vs.  $q$  rela-

tionship of the resampled data points. We repeat these 1000 times, and use the range between 16th- and 84th-percentiles as  $1-\sigma$  uncertainty.

To begin, as the first column of Figure 3 shows, in the youngest age bin,  $\sigma'_{\text{star}}$  decreases with increasing  $q$ , which is observed in both mass bins. This suggests that massive galaxies – regardless of their masses – still retain significant rotation in the aftermath of quenching. As they continue evolving and become older (the second and third columns of Figure 3), the relationship between  $\sigma'_{\text{star}}$  and  $q$  starts to differ in the two mass bins.

For low-mass quiescent galaxies with  $M_* < 10^{11.3}M_\odot$  (the first row of Figure 3),  $\sigma'_{\text{star}}$  decreases with  $q$  in all age bins, suggesting quiescent galaxies in this mass regime continue to retain significant rotation even long time after quenching. Overall, the median relationships between  $\sigma'_{\text{star}}$  and  $q$  are statistically consistent with each other for all age bins within the uncertainties, although there is some evidence that younger galaxies have a steeper relationship than the older ones.

For high-mass quiescent galaxies with  $M_* > 10^{11.3}M_\odot$  (the second row of Figure 3), the decreasing trend of  $\sigma'_{\text{star}}$  with  $q$  becomes significantly flattened as they become older. This shows that post-quenching dynamical transformations (1) happen in these very massive systems, which significantly reduce the amount of rotation and (2) these transformations are more profound in more massive quiescent galaxies.

In the analysis above we divided the low- and high-mass subsamples into only three age bins. We continue to study the variation of the  $\sigma'_{\text{star}}-q$  relationship by dividing the subsamples into more age bins. Specifically, instead of binning the subsamples using arbitrary bins of stellar age, we first sort stellar ages of individual galaxies into an increasing order. And starting from the first 30% of the sorted subsamples, we measure the Spearman’s rank correlation coefficient  $\rho$ . Then, we keep adding older quiescent galaxies into the correlation test, and study the change of  $\rho$  as a function of the maximum age of the galaxies included in the measure. The uncertainty of  $\rho$  calculated in this way is estimated by bootstrapping the sample galaxies 1000 times, and during each bootstrapping iteration we also resample the values of  $\sigma'_{\text{star}}$  and  $q$  with their corresponding measurement uncertainties using Gaussian distributions.

In Figure 4,  $\rho$  is plotted against the maximum mass-weighted age of the quiescent galaxies included to the Spearman’s rank correlation test. For galaxies that are freshly quenched, i.e. with relatively young stellar ages, we find a strong negative ( $\rho \sim -0.5$ , i.e. a decreasing trend) correlation between  $\sigma'_{\text{star}}$  and  $q$ , regardless of stellar mass. As older quiescent galaxies are added to the

<sup>3</sup> [www.statsmodels.org/dev/generated/statsmodels.nonparametric.smoothers\\_lowess.lowess.html](http://www.statsmodels.org/dev/generated/statsmodels.nonparametric.smoothers_lowess.lowess.html)

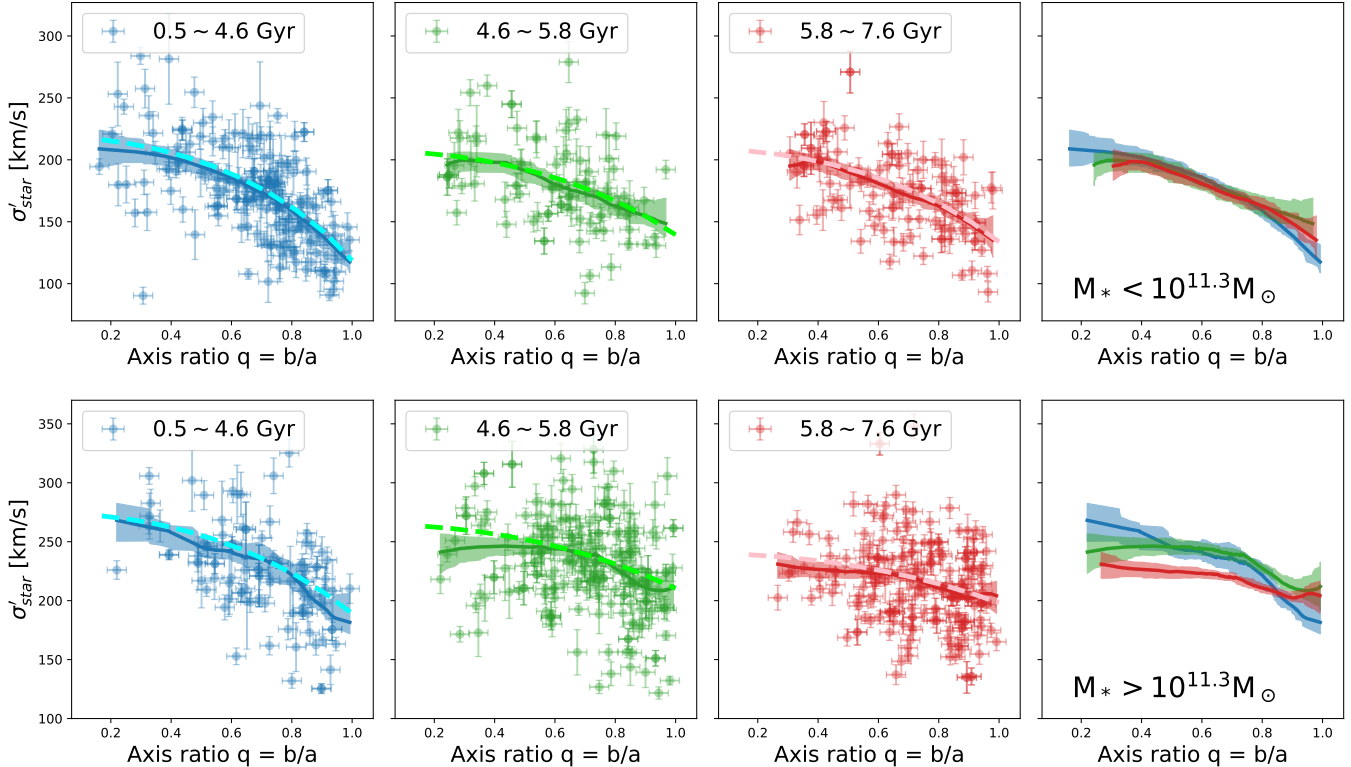


**Figure 3.**  $\sigma'_{\text{star}}$  vs.  $q$ . The first and second rows show the results of the quiescent galaxies with  $M_* < 10^{11.3}M_{\odot}$  and  $M_* > 10^{11.3}M_{\odot}$ , respectively. For each stellar-mass bin, galaxies are further divided into three age bins, each of which roughly contains 1/3 of the entire sample. In each panel the solid line and shaded region show the median trend and the corresponding 1- $\sigma$  uncertainty derived using the LOWESS algorithm. The dashed line shows the best-fit from our toy model (see Section 4.2). In the fourth column, all LOWESS median trends are shown together.

correlation test,  $\rho$  gradually changes from  $-0.5$  to  $-0.3$  for the high-mass ( $> 10^{11.3}M_{\odot}$ ) quiescent populations, while it remains approximately unchanged for the low-mass ones. This shows that the variation of the  $\sigma'_{\text{star}}$  vs.  $q$  relationship with age is significantly stronger in more massive quiescent galaxies, confirming the conclusion reached above based on Figure 3.

#### 4.2. A toy model for the $\sigma'_{\text{star}}$ vs. $q$ relationship

We now introduce a simple toy model, in an attempt to quantify the contribution from rotation to the observed relationship between  $\sigma'_{\text{star}}$  and  $q$ .

As detailed already in Section 1, both random and ordered motions contribute to  $\sigma'_{\text{star}}$ , which can be expressed as

$$(\sigma'_{\text{star}})^2 = \sigma^2 + \sigma_{\text{rotation}}^2 = \sigma^2 \left( 1 + \gamma^2 \left( \frac{V}{\sigma} \right)^2 \sin^2 i \right). \quad (1)$$

In the above equation we have used  $\sigma_{\text{rotation}} = \gamma V \sin i$ , which describes velocity dispersion observed through a slit (i.e. unresolved spectroscopy) due to a purely rotating disk, where  $V$  is the rotational velocity,  $i$  is the

inclination and  $\gamma$  is the conversion factor. Because to our knowledge there is no direct, statistical estimate of  $\gamma$  at high redshifts, we decide to fix  $\gamma = 0.7$  which is the median value from Cappellari et al. (2013) who measured it using the spatially resolved stellar kinematics of  $z \sim 0$  early type galaxies from ATLAS<sup>3D</sup>. The inclination can be estimated using  $q$  as

$$\sin i = \sqrt{\frac{1-q}{1-q_z}} \quad (2)$$

where  $q_z$  is the thickness of a disk which – following Belli et al. (2017) – we fix to be  $q_z = 0.2$ , namely about the minimum axis ratio observed in large extragalactic imaging surveys. The remaining unknowns in Equation 1 are  $\sigma$  and  $V$  (or  $V/\sigma$ ) that we attempt to constrain by fitting Equation 1 to the observed  $\sigma'_{\text{star}}$  vs.  $q$  relationship. To estimate the uncertainties of the fitted parameters, we use the same Monte Carlo method mentioned above by resampling the  $\sigma'_{\text{star}}$  and  $q$  measures using their uncertainties.

The best-fit relationships are plotted as dashed lines in Figure 3. The observations can be reproduced very well

with the toy model. The best-fit models are in excellent agreement with the LOWESS median trends.

In Figure 5, the inferred  $V/\sigma$  is plotted as a function of stellar age. Regardless of stellar age, the  $V/\sigma$  of the quiescent galaxies with  $M_* < 10^{11.3}M_\odot$  is greater than 1. As the population evolves, the  $V/\sigma$  of these systems decreases from  $2.3 \pm 0.3$  to  $1.7 \pm 0.4$ , implying that they remain rotationally supported, with  $V/\sigma \sim 1.7$ , even at least 7 Gyr after their formation<sup>4</sup>. In contrast, during the same cosmic time, the  $V/\sigma$  of the higher-mass quiescent galaxies with  $M_* > 10^{11.3}M_\odot$  monotonically decreases, from  $1.6 \pm 0.3$  (rotationally supported) to  $1.0 \pm 0.3$  (velocity dispersion supported), with increasing stellar age.

Before moving forward, we note several caveats of the  $V/\sigma$  inferred from our simple model. The misalignment between the slit and the kinematic major axis of galaxies has not been taken into account in our analysis. Neglecting this effect, however – given the large sample size of this study – should lead to an equal/similar systematic error in all subgroups and hence may not cause any substantial impacts on our conclusions, which only rely on a differential comparison. Also, the uncertainty on the value of  $\gamma$  in Equation 1 affects the inferred  $V/\sigma$ , a situation which, unfortunately, cannot be addressed at the moment. However, we note that the  $\gamma$  of gas kinematics has been statistically estimated at high redshifts and found to have a typical value of  $0.6 - 1$  (e.g., Weiner et al. 2006). Thus, while the adopted  $\gamma = 0.7$  is bracket by the range determined from high- $z$  gas kinematics, quantitatively the inferred  $V/\sigma$  presented in Figure 5 should be taken with caution. Qualitatively, however, our conclusions about the mass-dependent evolution of  $V/\sigma$  with stellar age should stand despite the over-simplified model. Finally, we also clarify that, when we state, e.g., that the quiescent population of a given stellar age is rotationally supported ( $V/\sigma > 1$ ), we do not mean that each one of the quiescent galaxies of that age bin retains significant rotation or that it has a disk, since the spatially integrated spectroscopy does not allow us to constrain that. Instead, what we really mean is that the quiescent *population* of that age *on average* should have significant rotation.

With the aforementioned caveats in mind, we now compare the inferred  $V/\sigma$  of this work with previous studies of the stellar kinematics in quiescent galaxies. Bezanson et al. (2018b) pioneered a LEGA-C study of

the dynamical transformation of  $z \sim 0.8$  massive quiescent galaxies using a small (relative to this study) sample of  $\sim 100$  galaxies whose major axes are overall aligned with the slit ( $|\text{PA}| < 45^\circ$ ), which allows spatially resolved analysis of stellar kinematics. They found that the most massive ( $> 10^{11.3}M_\odot$ ) quiescent galaxies show much less rotation compared to less massive systems. In broad agreement<sup>5</sup> with Bezanson et al. (2018b), our model suggests that quiescent populations of  $M_* > 10^{11.3}M_\odot$  are significantly less rotationally supported compared to the lower-mass ones, with  $V/\sigma = 1.2 \pm 0.1$  for the high-mass subsample compared to  $V/\sigma = 2.0 \pm 0.2$  for the low-mass one. The  $\approx 10\times$  larger in sample size of this study allows us to further group galaxies according to their stellar ages, adding a new piece of information regarding the dynamical transformation of quiescent galaxies as they evolve.

We also compare our inferred  $V/\sigma$  with the very limited number of direct  $V/\sigma$  measures at higher redshifts  $z \sim 2$ . In Figure 5, we show the results from Newman et al. (2018) who measured the stellar kinematics in three strongly lensed massive quiescent galaxies with  $M_* \gtrsim 10^{11.3}M_\odot$  at  $z \sim 2$  using spatially resolved spectroscopy. On average, those  $z \sim 2$  quiescent systems have even higher  $V/\sigma$  than that inferred for the youngest  $z \sim 0.8$  quiescent populations of similar masses ( $\gtrsim 10^{11.3}M_\odot$ ). Note that the median stellar age of the youngest bin of our  $z \sim 0.8$  sample is  $\sim 3 - 4$  Gyr which is longer than the Hubble time of  $z \sim 2$  (i.e.  $\sim 3$  Gyr). Thus, those  $z \sim 2$  quiescent galaxies must be – on average – younger (i.e. more freshly quenched) than the youngest quiescent populations considered in this study. If the dynamical state of the three lensed quiescent systems considered by Newman et al. (2018) is representative of the stellar kinematics of the entire quiescent populations at  $z \sim 2$  of comparable stellar mass, the implication is that the loss of angular momentum continuously and gradually happens after the cessation of star formation (quenching) in very massive ( $M_* \gtrsim 10^{11.3}M_\odot$ ) galaxies, transforming them from fast rotators right after quenching to slow rotators in at least  $\sim 7$  Gyr after their quenching.

## 5. DISCUSSION AND SUMMARY

To summarize, we studied the relationship between the dynamical transformation and quenching using the unresolved stellar kinematics of a sample of 952 massive

<sup>4</sup> Note that we do not know the quenching time of the sample galaxies. But, statistically, at a fixed redshift quiescent galaxies formed earlier, i.e. having older stellar ages, should also quench earlier.

<sup>5</sup> We do not directly compare our inferred  $V/\sigma$  with that of Bezanson et al. (2018b), because with spatially resolved analysis they were able to measure  $V_5/\sigma$  where  $V_5$  is the rotation velocity at 5 kpc that we are unable to constrain.

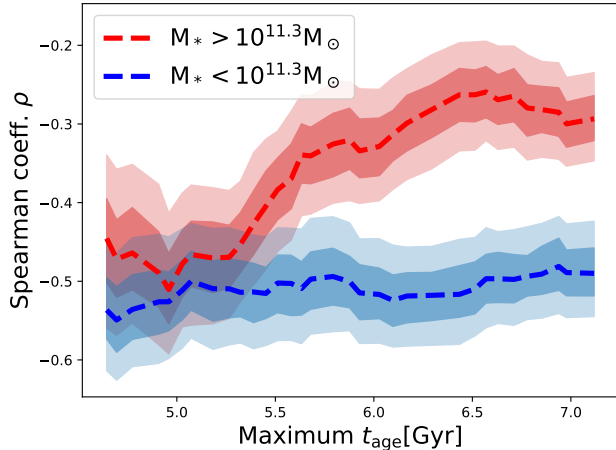


**Figure 4.** Change of the Spearman’s rank correlation coefficient as older quiescent galaxies are included to the correlation test (dashed lines). The  $x$ -axis shows the maximum mass-weighted age of the quiescent galaxies included in the test. The dark and light shaded regions mark the 0.5- and 1- $\sigma$  uncertainties.

( $> 10^{10.5} M_{\odot}$ ) quiescent galaxies at  $0.6 < z < 1$  from the LEGA-C survey. Using the SED fitting code PROSPECTOR, we robustly measured the stellar-population properties of the sample galaxies. We focused on the variation of the relationship between  $\sigma'_{\text{star}}$  and  $q$  as a function of stellar age, and of stellar mass.

We found a decreasing trend of  $\sigma'_{\text{star}}$  with  $q$  for the youngest quiescent galaxies of all masses. The implication is that freshly quenched galaxies, regardless of stellar mass, still have significant rotation. This is strong evidence that the occurrence of quenching in itself at high redshift does not *fully* transform massive galaxies into dispersion supported systems as it takes place or immediately after. Based on what we have found in our recent study (Ji & Giavalisco 2022b), however, it is very likely that quenching happens in close temporal proximity to whatever mechanism alters the inner structure of galaxies by building dense central stellar cores.

We found that the post-quenching dynamical transformation of quiescent galaxies depends on stellar mass, adding an important piece of information regarding the early formation epoch of fast and slow rotators. We remind that  $M_* = 10^{11.3} M_{\odot}$  is the characteristic mass that separates the fast and slow rotators at  $z \sim 0$  (Cappellari 2016). For very massive galaxies, with  $M_* > 10^{11.3} M_{\odot}$ , at  $z \sim 0.8$ , we observe that the incidence of rotational support gradually reduces, as the galaxies become older. Using a simple toy model, we infer these very massive systems transform from being rotationally supported in the aftermath of quenching, with  $V/\sigma \sim 1.6$ , to being velocity-dispersion supported  $\approx 7$

Gyr after their formation, with  $V/\sigma \sim 1.0$ . In contrast, lower-mass quiescent populations with  $M_* < 10^{11.3} M_{\odot}$  show a much weaker post-quenching dynamical evolution. Even 7 Gyr after their formation, these lower-mass quiescent systems still retain significant rotation with  $V/\sigma \sim 1.7$ .

Our findings are consistent with the picture that quiescent galaxies at the high-mass end formed in dense environments, presumably in the regions with large overdensities of the primordial density field. After quenching, these very massive galaxies continue changing their dynamical states via continuous gas accretion or incoherent merging with other adjacent galaxies through dynamic friction. These very massive systems will eventually evolve into slow rotators seen at  $z \sim 0$ , because multiple incoherent merging episodes can cause significant loss of angular momentum (e.g. Emsellem et al. 2011). For lower-mass quiescent galaxies, however, they very likely formed in regions with, comparatively speaking, smaller overdensities, meaning that they have shallower gravitational wells such that the frequency of merging events with other smaller galaxies is much lower than that in more massive halos. Consequently, lower-mass quiescent galaxies can retain significant rotations long time after their formation, i.e. they will evolve into fast rotators.

The mass-dependent evolution of massive quiescent galaxies has been revealed in both their morphological (e.g. van der Wel et al. 2014; Ji & Giavalisco 2022a; Ji et al. 2024) and chemical properties (e.g. Kriek et al. 2019; Jafariyazani et al. 2020; Cheng et al. 2024; Beverage et al. 2024) in the high- $z$  Universe. The purely empirical study presented here, which uses unresolved spectroscopy, provides robust evidence that, statistically, the evolution of the dynamical properties (angular momentum in particular) of quiescent galaxies also depends on stellar mass. In other words, we are witnessing the early build-up of the populations of fast and slow rotators at  $z \sim 0.8$ , when the Universe was only half of its age nowadays.

Undoubtedly, future spatially resolved spectroscopy of individual targets is needed to fully characterize the dispersion and intrinsic distribution of the dynamical state of massive quiescent galaxies and their evolution across cosmic time, including the mechanisms responsible for the dichotomy of stellar kinematics found in  $z \sim 0$  early type galaxies. Yet, results of the empirical study presented here, and its simplicity, provides robust evidence that the formation of the dichotomy was well underway at half the Hubble time.



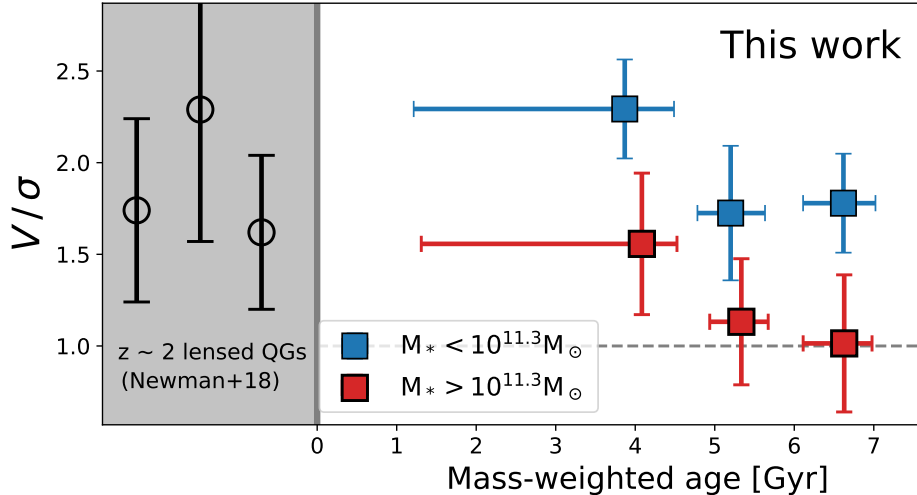


**Figure 5.**  $V/\sigma$  as a function of stellar age. Blue ( $M_* < 10^{11.3} M_\odot$ ) and red ( $M_* > 10^{11.3} M_\odot$ ) squares show the  $V/\sigma$ , inferred from our toy model (Section 4.2), of  $z \sim 0.8$  quiescent populations of different ages. The horizontal dashed line marks  $V/\sigma = 1$ . In the left-most grey shaded region, we also plot three strongly lensed massive ( $\gtrsim 10^{11.3} M_\odot$ ) quiescent galaxies at  $z \sim 2$  with direct, spatially resolved measures of stellar kinematics from Newman et al. (2018).

- 1 This work was completed in part with resources provided by the Green High Performance Computing
- 2 Cluster (GHPCC) of the University of Massachusetts
- 3 Amherst.

*Software:* Prospector (Johnson et al. 2021), FSPS (Conroy et al. 2009; Conroy & Gunn 2010), MIST (Choi et al. 2016; Dotter 2016), MILES (Falc3n-Barroso et al. 2011), GALFIT (Peng et al. 2010)

## APPENDIX

### A. TESTING THE ROBUSTNESS OF THE STELLAR-AGE INFERENCE

Here we present and discuss in detail about our tests on the stellar-age measures from our PROSPECTOR fitting.

To begin, we compare the best-fit SED models predicted by PROSPECTOR with the observed LEGA-C spectra. Specifically, we compare the median observed and predicted spectra of each one of the subgroups presented in the main text (Section 4). We remind that our PROSPECTOR fitting only used photometric data ( $\approx 40$  bands), i.e. the spectra were not used in the SED modeling. This comparison thus allows us to have a direct and broad view on the quality of our SED fitting.

As Figure 6 shows, the median spectra of all subgroups dim at the rest-frame UV wavelengths, and show strong stellar absorption features without any strong emission lines over rest-frame  $3800 - 5200 \text{ \AA}$ , which demonstrates, once again, the effectiveness of the UVJ technique in identifying quiescent galaxies. The the best-fit spectra from SED modeling are in excellent agreement with the observed ones, within the uncertainties, for all subgroups. Moreover, as the right-most panel of Figure 6 shows, galaxies with older stellar ages – inferred from PROSPECTOR – also have redder observed spectra, even though the spectral information was not included during the SED fitting procedure. This agreement suggests that the stellar-age inference from our SED fitting procedure is robust. We stress, however, that the conclusion above *does not at all* imply that the spectral information is not needed for SED fitting. In fact, robust measurements of metallicity and elemental abundance are only possible with spectra. What we really mean is that the stellar age of high- $z$  quiescent galaxies can be inferred robustly when densely-sampled, panchromatic photometry is available. Similar conclusions were also reached by Ji & Giavalisco (2022a) using synthetic galaxies from cosmological simulations.

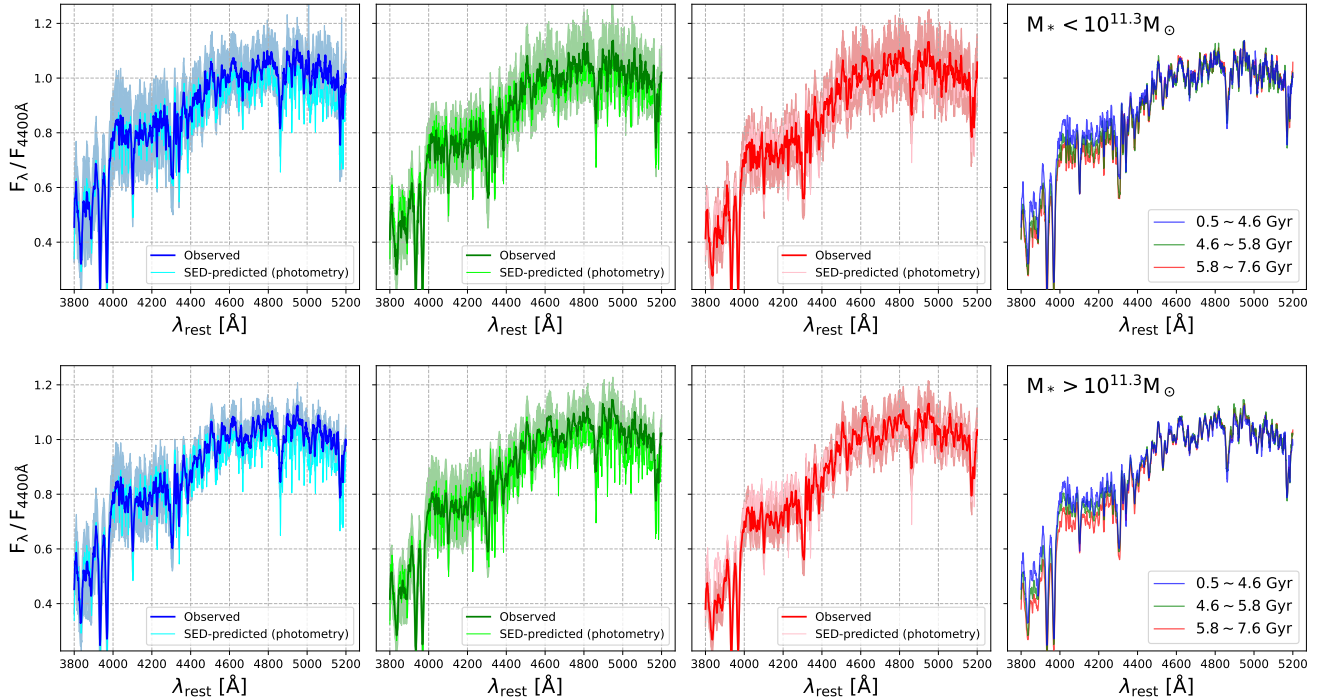


**Figure 6.** Comparison between the median observed (LEGA-C) and predicted (PROSPECTOR fitting with photometry only) spectra of each one of the subgroups discussed in the main text. The sample division here is the same as used in Figure 3. In each panel, we also show the  $1\text{-}\sigma$  range (standard deviation) of the observed spectrum as shaded region. In the right-most panel, the median observed spectra of all stellar age bins are shown together.

Despite the numerous advantages of fitting photometric and spectral data simultaneously (e.g., Tacchella et al. 2022), here we want to highlight one potential, serious systematic: the non-trivial aperture matching that is required when combining photometry and spectroscopy. To tackle this, most studies simply rescale (or perform the fit with the rescaling factor as a free parameter) the observed spectra to the same flux level of photometry. The big assumption behind such a procedure is that there is no strong color/stellar-population variation between the photometric aperture and the spectral slit. This assumption can be problematic given that color gradients have been clearly observed in high- $z$  massive quiescent galaxies (e.g. Suess et al. 2020; Ji et al. 2024). Ideally, in order to simultaneously fitting photometry and spectroscopy, one needs forward modeling the instrumental effects to properly account for e.g. the mismatch of apertures, which however is beyond the scope of this work. The fact that the predicted spectra using photometry alone are in very good agreement with the observed ones provides confidence that the measures of stellar age of the sample galaxies are robust.

We continue our tests on the stellar-age measures by comparing the age-color relationship from our PROSPECTOR fitting with earlier studies. Whitaker et al. (2013) stacked the 3D-HST grism spectra of massive quiescent galaxies at  $z \sim 2$ , and fit the stacked spectral features with a solar-metallicity, single stellar population model. They found that quiescent galaxies having bluer rest-frame ( $U - V$ ) and ( $V - J$ ) colors are younger than those having the redder colors. We made a similar comparison and found excellent qualitative agreement, as we show in Figure 7.

Similarly, Belli et al. (2019) derived and calibrated the relationship between stellar age and rest-frame UVJ colors using a sample of 24 quiescent galaxies at  $1.5 < z < 2.5$  with deep rest-optical spectroscopy. The stellar ages of their sample galaxies were estimated by modeling spectra and photometry combined. To assess the consistency between their results and ours, we compare the relationship between stellar age and UVJ colors of our measurements with that of Belli et al. (2019). To do so, we first derive the quiescent sequence of our sample by conducting a linear regression between the ( $U - V$ ) and ( $V - J$ ) colors. With the best-fit linear relationship between the two colors in hand, we use Equation 3 of Belli et al. (2019)<sup>6</sup> to derive the expected change of stellar age along our quiescent sequence, which is

<sup>6</sup>  $\log(\text{Age}/\text{yr}) = 7.03 + 0.84(V - J) + 0.74(U - V)$

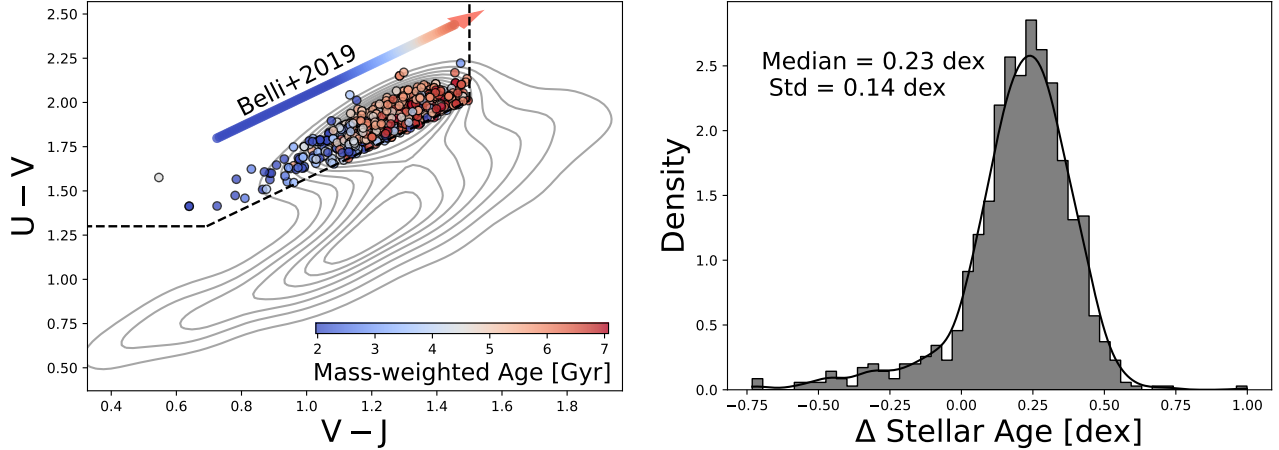


**Figure 7. Left:** UVJ diagram. The quiescent galaxies of this study are shown as individual circles color coded according to stellar ages from our PROSPECTOR fitting. The background contours show the distribution of all LEGA-C galaxies with  $M_* > 10^{10.5} M_\odot$ . The black dashed lines mark the UVJ selection criteria of Muzzin et al. (2013). The vector shows the best-fit relation between the stellar age and UVJ colors from Belli et al. (2019). Great qualitative agreement – galaxies with bluer UVJ colors are younger – is seen between the two stellar age inferences. **Right:** Distribution of the difference in stellar age between our PROSPECTOR measurements and those inferred using the best-fit relation of Belli et al. (2019). Our measurements on average return a  $0.23 \pm 0.14$  dex older stellar age.

shown as the vector in Figure 7. We run a Pearson correlation test between the stellar ages from PROSPECTOR and the stellar ages inferred using the best-fit relation of Belli et al. (2019). We found a strong correlation, with Pearson coefficient  $r = 0.52$ , which demonstrates good qualitative agreement between our stellar-age measures and those of Belli et al. (2019). Note, however, that the above relationship (Belli et al. 2019) between age and rest-frame colors was derived at  $z \sim 1.7$ . As the galaxies age and their colors evolve, we expect the relationship to change as well. While the study of the color evolution of quiescent galaxies is beyond the scope of this work, we note that, as the right panel of Figure 7 shows, a systematic age difference is observed between our measures with PROSPECTOR at  $z \sim 0.8$  and those of Belli et al. (2019) at  $z \sim 1.7$  such that the  $z \sim 0.8$  galaxies are older than those at  $z \sim 1.7$  by 0.23 dex, or 2.6 Gyr which is about the time interval between the two redshifts,  $t_H^{z=0.8} - t_H^{z=1.7} \approx 2.9$  Gyr.

In summary, by comparing (1) the predicted spectra from PROSPECTOR with the observed ones from LEGA-C and (2) the stellar ages from PROSPECTOR and the ones inferred using the age-color relationship reported by previous studies, we showed very good agreement among different stellar-age measures. We stress that, because the conclusions of this study only depend on differential stellar-age measures (younger vs. older), rather than absolute stellar-age determinations, we conclude that the results and key conclusions presented in this study are robust.

## REFERENCES

- Balogh, M. L., Morris, S. L., Yee, H. K. C., Carlberg, R. G., & Ellingson, E. 1999, *ApJ*, 527, 54, doi: [10.1086/308056](https://doi.org/10.1086/308056)
- Belli, S., Newman, A. B., & Ellis, R. S. 2017, *ApJ*, 834, 18, doi: [10.3847/1538-4357/834/1/18](https://doi.org/10.3847/1538-4357/834/1/18)
- . 2019, *ApJ*, 874, 17, doi: [10.3847/1538-4357/ab07af](https://doi.org/10.3847/1538-4357/ab07af)
- Beverage, A. G., Kriek, M., Suess, K. A., et al. 2024, *ApJ*, 966, 234, doi: [10.3847/1538-4357/ad372d](https://doi.org/10.3847/1538-4357/ad372d)
- Bezanson, R., van der Wel, A., Straatman, C., et al. 2018a, *ApJL*, 868, L36, doi: [10.3847/2041-8213/aaf16b](https://doi.org/10.3847/2041-8213/aaf16b)
- Bezanson, R., van der Wel, A., Pacifici, C., et al. 2018b, *ApJ*, 858, 60, doi: [10.3847/1538-4357/aabc55](https://doi.org/10.3847/1538-4357/aabc55)
- Byler, N., Dalcanton, J. J., Conroy, C., & Johnson, B. D. 2017, *ApJ*, 840, 44, doi: [10.3847/1538-4357/aa6c66](https://doi.org/10.3847/1538-4357/aa6c66)
- Calzetti, D., Armus, L., Bohlin, R. C., et al. 2000, *ApJ*, 533, 682, doi: [10.1086/308692](https://doi.org/10.1086/308692)
- Cappellari, M. 2016, *ARA&A*, 54, 597, doi: [10.1146/annurev-astro-082214-122432](https://doi.org/10.1146/annurev-astro-082214-122432)
- . 2017, *MNRAS*, 466, 798, doi: [10.1093/mnras/stw3020](https://doi.org/10.1093/mnras/stw3020)
- Cappellari, M., Emsellem, E., Bacon, R., et al. 2007, *MNRAS*, 379, 418, doi: [10.1111/j.1365-2966.2007.11963.x](https://doi.org/10.1111/j.1365-2966.2007.11963.x)
- Cappellari, M., Scott, N., Alatalo, K., et al. 2013, *MNRAS*, 432, 1709, doi: [10.1093/mnras/stt562](https://doi.org/10.1093/mnras/stt562)

- Carnall, A. C., Leja, J., Johnson, B. D., et al. 2019, *ApJ*, 873, 44, doi: [10.3847/1538-4357/ab04a2](https://doi.org/10.3847/1538-4357/ab04a2)
- Cheng, C. M., Kriek, M., Beverage, A. G., et al. 2024, *MNRAS*, 532, 3604, doi: [10.1093/mnras/stae1739](https://doi.org/10.1093/mnras/stae1739)
- Choi, J., Dotter, A., Conroy, C., et al. 2016, *ApJ*, 823, 102, doi: [10.3847/0004-637X/823/2/102](https://doi.org/10.3847/0004-637X/823/2/102)
- Conroy, C., & Gunn, J. E. 2010, *ApJ*, 712, 833, doi: [10.1088/0004-637X/712/2/833](https://doi.org/10.1088/0004-637X/712/2/833)
- Conroy, C., Gunn, J. E., & White, M. 2009, *ApJ*, 699, 486, doi: [10.1088/0004-637X/699/1/486](https://doi.org/10.1088/0004-637X/699/1/486)
- D'Eugenio, F., Perez-Gonzalez, P., Maiolino, R., et al. 2023, arXiv e-prints, arXiv:2308.06317, doi: [10.48550/arXiv.2308.06317](https://doi.org/10.48550/arXiv.2308.06317)
- Dotter, A. 2016, *ApJS*, 222, 8, doi: [10.3847/0067-0049/222/1/8](https://doi.org/10.3847/0067-0049/222/1/8)
- Emsellem, E., Cappellari, M., Peletier, R. F., et al. 2004, *MNRAS*, 352, 721, doi: [10.1111/j.1365-2966.2004.07948.x](https://doi.org/10.1111/j.1365-2966.2004.07948.x)
- Emsellem, E., Cappellari, M., Krajnović, D., et al. 2007, *MNRAS*, 379, 401, doi: [10.1111/j.1365-2966.2007.11752.x](https://doi.org/10.1111/j.1365-2966.2007.11752.x)
- . 2011, *MNRAS*, 414, 888, doi: [10.1111/j.1365-2966.2011.18496.x](https://doi.org/10.1111/j.1365-2966.2011.18496.x)
- Falcón-Barroso, J., Sánchez-Blázquez, P., Vazdekis, A., et al. 2011, *A&A*, 532, A95, doi: [10.1051/0004-6361/201116842](https://doi.org/10.1051/0004-6361/201116842)
- Gardner, J. P., Mather, J. C., Abbott, R., et al. 2023, *PASP*, 135, 068001, doi: [10.1088/1538-3873/acd1b5](https://doi.org/10.1088/1538-3873/acd1b5)
- Jafariyazani, M., Newman, A. B., Mobasher, B., et al. 2020, *ApJL*, 897, L42, doi: [10.3847/2041-8213/aba11c](https://doi.org/10.3847/2041-8213/aba11c)
- Jakobsen, P., Ferruit, P., Alves de Oliveira, C., et al. 2022, *A&A*, 661, A80, doi: [10.1051/0004-6361/202142663](https://doi.org/10.1051/0004-6361/202142663)
- Ji, Z., & Gialalisco, M. 2022a, arXiv e-prints, arXiv:2204.02414. <https://arxiv.org/abs/2204.02414>
- . 2022b, arXiv e-prints, arXiv:2208.04325. <https://arxiv.org/abs/2208.04325>
- Ji, Z., Gialalisco, M., Williams, C. C., et al. 2018, *ApJ*, 862, 135, doi: [10.3847/1538-4357/aacc2c](https://doi.org/10.3847/1538-4357/aacc2c)
- Ji, Z., Williams, C. C., Suess, K. A., et al. 2024, arXiv e-prints, arXiv:2401.00934, doi: [10.48550/arXiv.2401.00934](https://doi.org/10.48550/arXiv.2401.00934)
- Johnson, B. D., Leja, J., Conroy, C., & Speagle, J. S. 2021, *ApJS*, 254, 22, doi: [10.3847/1538-4365/abef67](https://doi.org/10.3847/1538-4365/abef67)
- Kauffmann, G., Heckman, T. M., White, S. D. M., et al. 2003, *MNRAS*, 341, 54, doi: [10.1046/j.1365-8711.2003.06292.x](https://doi.org/10.1046/j.1365-8711.2003.06292.x)
- Kriek, M., Price, S. H., Conroy, C., et al. 2019, *ApJL*, 880, L31, doi: [10.3847/2041-8213/ab2e75](https://doi.org/10.3847/2041-8213/ab2e75)
- Kroupa, P. 2001, *MNRAS*, 322, 231, doi: [10.1046/j.1365-8711.2001.04022.x](https://doi.org/10.1046/j.1365-8711.2001.04022.x)
- Laigle, C., McCracken, H. J., Ilbert, O., et al. 2016, *ApJS*, 224, 24, doi: [10.3847/0067-0049/224/2/24](https://doi.org/10.3847/0067-0049/224/2/24)
- Leja, J., Carnall, A. C., Johnson, B. D., Conroy, C., & Speagle, J. S. 2019, *ApJ*, 876, 3, doi: [10.3847/1538-4357/ab133c](https://doi.org/10.3847/1538-4357/ab133c)
- Leja, J., Johnson, B. D., Conroy, C., van Dokkum, P. G., & Byler, N. 2017, *ApJ*, 837, 170, doi: [10.3847/1538-4357/aa5ffe](https://doi.org/10.3847/1538-4357/aa5ffe)
- Leja, J., Speagle, J. S., Ting, Y.-S., et al. 2022, *ApJ*, 936, 165, doi: [10.3847/1538-4357/ac887d](https://doi.org/10.3847/1538-4357/ac887d)
- Muzzin, A., Marchesini, D., Stefanon, M., et al. 2013, *ApJ*, 777, 18, doi: [10.1088/0004-637X/777/1/18](https://doi.org/10.1088/0004-637X/777/1/18)
- Nanayakkara, T., Esdaile, J., Glazebrook, K., et al. 2022, *PASA*, 39, e002, doi: [10.1017/pasa.2021.61](https://doi.org/10.1017/pasa.2021.61)
- Newman, A. B., Belli, S., & Ellis, R. S. 2015, *ApJL*, 813, L7, doi: [10.1088/2041-8205/813/1/L7](https://doi.org/10.1088/2041-8205/813/1/L7)
- Newman, A. B., Belli, S., Ellis, R. S., & Patel, S. G. 2018, *ApJ*, 862, 126, doi: [10.3847/1538-4357/aacd4f](https://doi.org/10.3847/1538-4357/aacd4f)
- Peng, C. Y., Ho, L. C., Impey, C. D., & Rix, H.-W. 2010, *AJ*, 139, 2097, doi: [10.1088/0004-6256/139/6/2097](https://doi.org/10.1088/0004-6256/139/6/2097)
- Planck Collaboration, Aghanim, N., Akrami, Y., et al. 2020, *A&A*, 641, A6, doi: [10.1051/0004-6361/201833910](https://doi.org/10.1051/0004-6361/201833910)
- Straatman, C. M. S., van der Wel, A., Bezanson, R., et al. 2018, *ApJS*, 239, 27, doi: [10.3847/1538-4365/aae37a](https://doi.org/10.3847/1538-4365/aae37a)
- Suess, K. A., Kriek, M., Price, S. H., & Barro, G. 2020, *ApJL*, 899, L26, doi: [10.3847/2041-8213/abacc9](https://doi.org/10.3847/2041-8213/abacc9)
- Tacchella, S., Conroy, C., Faber, S. M., et al. 2022, *ApJ*, 926, 134, doi: [10.3847/1538-4357/ac449b](https://doi.org/10.3847/1538-4357/ac449b)
- Toft, S., Zabl, J., Richard, J., et al. 2017, *Nature*, 546, 510, doi: [10.1038/nature22388](https://doi.org/10.1038/nature22388)
- van der Wel, A., Bell, E. F., Häussler, B., et al. 2012, *ApJS*, 203, 24, doi: [10.1088/0067-0049/203/2/24](https://doi.org/10.1088/0067-0049/203/2/24)
- van der Wel, A., Franx, M., van Dokkum, P. G., et al. 2014, *ApJ*, 788, 28, doi: [10.1088/0004-637X/788/1/28](https://doi.org/10.1088/0004-637X/788/1/28)
- van der Wel, A., Noeske, K., Bezanson, R., et al. 2016, *ApJS*, 223, 29, doi: [10.3847/0067-0049/223/2/29](https://doi.org/10.3847/0067-0049/223/2/29)
- van der Wel, A., Bezanson, R., D'Eugenio, F., et al. 2021, *ApJS*, 256, 44, doi: [10.3847/1538-4365/ac1356](https://doi.org/10.3847/1538-4365/ac1356)
- Weaver, J. R., Kauffmann, O. B., Ilbert, O., et al. 2022, *ApJS*, 258, 11, doi: [10.3847/1538-4365/ac3078](https://doi.org/10.3847/1538-4365/ac3078)
- Weiner, B. J., Willmer, C. N. A., Faber, S. M., et al. 2006, *ApJ*, 653, 1027, doi: [10.1086/508921](https://doi.org/10.1086/508921)
- Whitaker, K. E., van Dokkum, P. G., Brammer, G., et al. 2013, *ApJL*, 770, L39, doi: [10.1088/2041-8205/770/2/L39](https://doi.org/10.1088/2041-8205/770/2/L39)
- Worthey, G., Faber, S. M., Gonzalez, J. J., & Burstein, D. 1994, *ApJS*, 94, 687, doi: [10.1086/192087](https://doi.org/10.1086/192087)
- Worthey, G., & Ottaviani, D. L. 1997, *ApJS*, 111, 377, doi: [10.1086/313021](https://doi.org/10.1086/313021)